

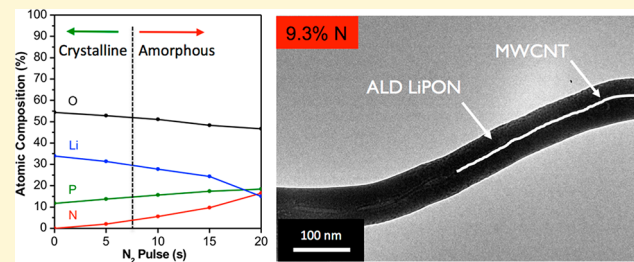
Atomic Layer Deposition of the Solid Electrolyte LiPON

Alexander C. Kozen,^{*†‡} Alexander J. Pearse,^{†‡} Chuan-Fu Lin,^{†‡} Malachi Noked,^{†‡} and Gary W. Rubloff^{†‡}

[†]Department of Materials Science & Engineering and [‡]Institute for Systems Research, University of Maryland, College Park, Maryland 20742, United States

Supporting Information

ABSTRACT: We demonstrate an atomic layer deposition (ALD) process for the solid electrolyte lithium phosphorous oxynitride (LiPON) using lithium *tert*-butoxide (LiO^{tBu}), H_2O , trimethylphosphate (TMP), and plasma N_2 ($^{\text{p}}\text{N}_2$) as precursors. We use in-situ spectroscopic ellipsometry to determine growth rates for process optimization to design a rational, quaternary precursor ALD process where only certain substrate–precursor chemical reactions are favorable. We demonstrate via in-situ XPS tunable nitrogen incorporation into the films by variation of the $^{\text{p}}\text{N}_2$ dose and find that ALD films over approximately 4.5% nitrogen are amorphous, whereas LiPON ALD films with less than 4.5% nitrogen are polycrystalline. Finally, we characterize the ionic conductivity of the ALD films as a function of nitrogen content and demonstrate their functionality on a model battery electrode—a Si anode on a Cu current collector.



While planar thin film solid-state microbatteries are in commercial production, the push for higher energy and power density necessitates development of 3D device geometries, realized by improvements in device fabrication processes.^{1,2} Moving from planar layer structures to high aspect ratio 3D electrode structures holds promise for significant power enhancement without much loss of energy density, or alternatively a tunable optimization and trade-off between power and energy to fit the application.

Since its discovery in the early 1990s,³ LiPON (lithium phosphorus oxynitride) has been one of the most popular solid state electrolytes used for planar lithium ion microbatteries. LiPON thin films are commonly deposited using reactive sputtering of a Li_3PO_4 target in an N_2 atmosphere.^{4–8} Generally, sputtered LiPON films are $\sim 1 \mu\text{m}$ thick, but sputtering of much thinner LiPON films (12 nm) has recently been demonstrated.⁹ As a physical deposition technique, sputtering is generally unable to deposit high quality films on 3D geometries.¹⁰ Also, the low reactivity of the N_2 gas during the sputtering process makes it difficult to dope these films with $> 2\%$ N.

Highly tunable N doping of LiPON is possible through e-beam evaporation of Li_3PO_4 coupled with a N_2 plasma discharge above the substrate;¹¹ however, this technique is also limited to planar substrates.

More recently, Kim et al. developed a MOCVD process for LiPON,¹² but the high deposition temperatures reported (500 °C) are undesirable for coprocessing with many battery materials and packaging components, precluding deposition on materials such as (i) Li_2CoO_3 cathodes without degradation during the deposition process or (ii) metallic Li metal anodes without melting them.

ALD has emerged as the premier deposition process for fabrication of uniform, thin, conformal films on high aspect ratio scaffolds,^{13–16} and ALD has previously been used to fabricate the solid electrolytes $(\text{Li},\text{La})_x\text{Ti}_y\text{O}_z$,¹⁷ Li_3PO_4 ,¹⁸ $\text{Li}_x\text{Al}_2\text{O}_3$,^{19,20} and $\text{Li}_x\text{Si}_y\text{Al}_2\text{O}_3$.²¹

Utilizing a unique integrated high-vacuum deposition, surface characterization, and battery assembly system,²² we have developed a quaternary ALD process for the solid electrolyte LiPON. We demonstrate tunable nitrogen doping by using N_2 plasma doses at a critical step during the ALD process, and we show the effect of the nitrogen content on the morphology of the deposited LiPON thin film.

EXPERIMENTAL PROCEDURES

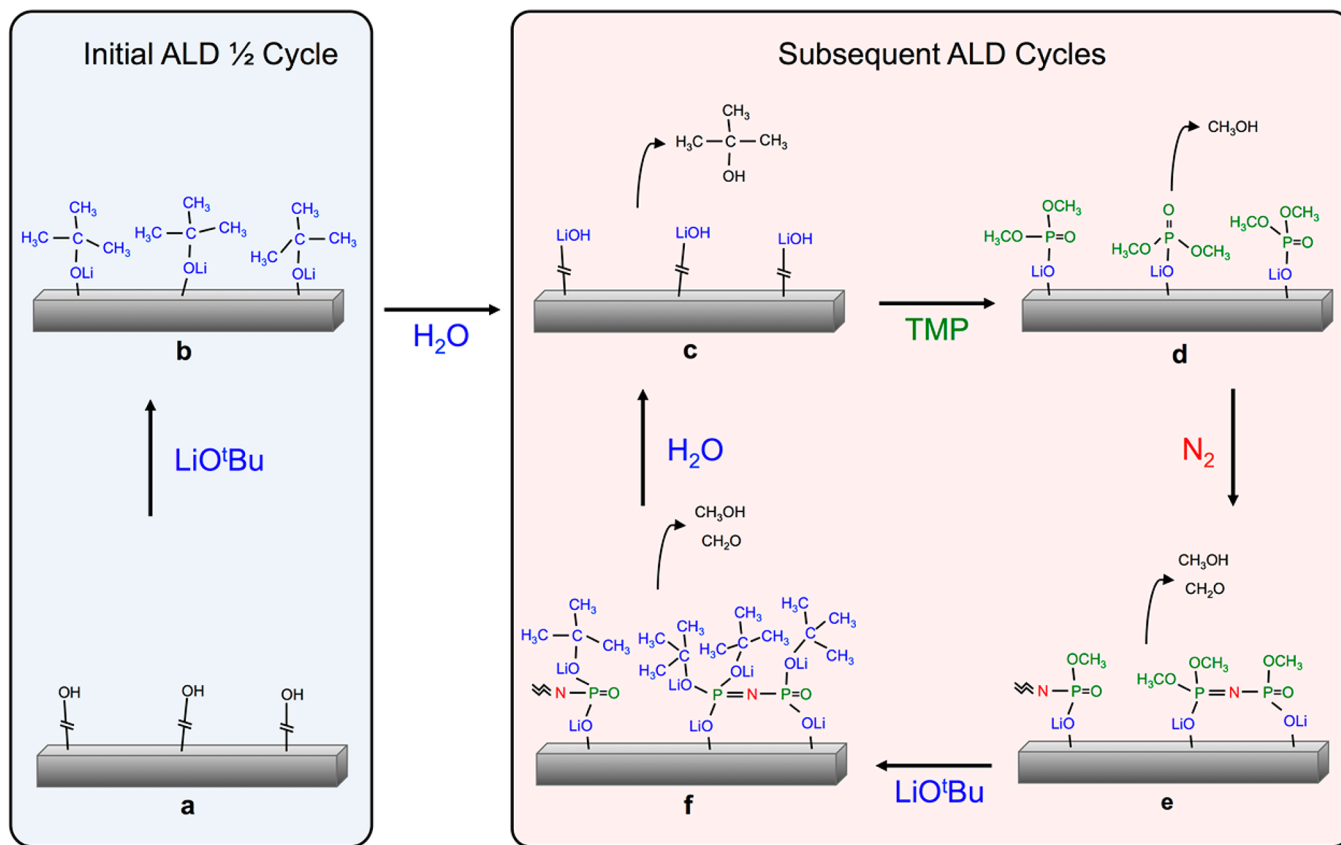
Silicon substrates were cleaned using a stepwise acetone, methanol, isopropanol rinse procedure, blown dry, and then pumped down in a UHV load lock chamber to a maximum pressure of $< 1 \times 10^{-7}$ Torr. Next, the substrates were transferred to an Ultratech Fiji F200, where we deposited the LiPON ALD films at 250 °C using the precursors lithium *tert*-butoxide (LiO^{tBu}) (Aldrich, 99.7%), deionized H_2O , trimethylphosphate (TMP) (Aldrich, 99.9%), and N_2 gas (Praxair, grade 5.0). Argon (Airgas, grade 4.9) was used as a carrier gas. The base pressure of the ALD reactor was $< 2 \times 10^{-6}$ Torr, and a process pressure of 200 mTorr was maintained via Ar gas flow. The solid LiO^{tBu} precursor was kept at 165 °C and was delivered to the ALD chamber using a bubbler with 40 sccm argon carrier gas flow. ALD films were deposited using precursor saturation doses of 3 s for the LiO^{tBu} , 0.06 s for the H_2O , and 0.4 s for the TMP with 30 s purges after each precursor dose. The $^{\text{p}}\text{N}_2$ pulse was varied from 5 s to 30 s at

Received: May 4, 2015

Revised: July 6, 2015

Published: July 9, 2015



Scheme 1. Cartoon of the Proposed ALD LiPON Process Chemistry^a

^a(a) Hydroxyl terminated substrate; (b) metastable surface after the LiO^tBu pulse; (c) H_2O pulse removes the *tert*-butanol ligands and forms LiOH on the surface; (d) TMP reacts with surface LiOH through ligand exchange reaction, evolving CH_3OH ; (e) N_2 plasma cross-links phosphorous atoms and evolve CH_3OH and CH_2O ; (f) LiO^tBu reacts with $-\text{OCH}_3$ ligands and evolves both CH_2OH and CH_2O . The initial LiO^tBu and H_2O pulses shown in (a) and (b) are required “activate” the substrate prior to deposition. For all subsequent ALD cycles, the process chemistry in (c) through (f) is repeated as one ALD cycle.

a 40 sccm flow rate and a plasma power of 300 W, and a 5 s purge step was included after the $^{\text{p}}\text{N}_2$. A growth rate of 1.05 Å/s was achieved for the LiPON ALD film as determined in-operando using a J.A. Woollam M-2000D spectroscopic ($\lambda = 193\text{--}1000$ nm) ellipsometer and a B-spline optical model.

Post-deposition, substrates were transferred under UHV from the ALD system to a Kratos Ultra DLD XPS system. Survey spectra were collected without charge neutralization using a 12 kV monochromatic Al $\text{K}\alpha$ X-ray source in hybrid lens mode with a step size of 1 eV and pass energy of 160 eV. High-resolution spectra were collected using a 12 kV monochromatic Al $\text{K}\alpha$ X-ray source in hybrid lens mode with a step size of 0.1 eV and pass energy of 20 eV. XPS data were analyzed using CasaXPS with peak area quantification normalized by standard photoionization cross sections corrected for our instrument geometry²³ and a Shirley background algorithm. Ex-situ AFM characterization was conducted using an NT-MDT NTEGRA Spectra system in tapping mode at a scan rate of 1 $\mu\text{m}/\text{s}$. SEM imaging was done with a Hitachi SU-70 microscope, and TEM imaging was done with a JEM 2100 LAB6 microscope.

For electrochemical characterization, ALD LiPON was deposited onto stainless steel substrates and transferred to our glovebox without air exposure. These films were assembled as the working electrode into CR2032 coin cells (MTI) with a Li metal (Alfa Aesar) counter electrode and 1 M LiPF_6 in 1:1 EC:DEC electrolyte (Novolyte). EIS and CV measurements were carried out using a Bio-Logic VSP potentiostat.

RESULTS AND DISCUSSION

There are two ways to consider quaternary ALD process development. First, quaternary process development can be seen as the combination of multiple constituent ALD processes in different ratios. For example, in our case this would be a combination of the Li_3PO_4 , Li_2O , and Li_xN ALD processes. Each of these individual materials is composed of two precursors (e.g., A + B, C + D, and E + F), and combining these constituent materials in different ratios of ALD supercycles can result in a degree of tunability in the resulting nanolaminates film.

However, this approach presents a few problems. First, if two of the constituent ALD materials use the same precursor, then this creates a precursor pulse redundancy during the process. Second, due to the surface termination of the films, some precursors may only be compatible with specific surface species, preventing the incorporation of elements into the resulting films due to differences in ligand exchange reaction energies. Lastly, in order to control film stoichiometry, different ratios of the constituent ALD precursors must be used, which can result in nanolaminates with an uneven distribution of constituent elements.

Instead, we take an additive synthesis approach to quaternary ALD process development, starting with the previously reported thermal ALD process for Li_2O .²⁴ From this process, we add an additional precursor, TMP, and determine the

saturation dose of the ternary Li_3PO_4 ALD process (not shown). Notably, use of the ternary (including water) ALD process instead of the previously published binary Li_3PO_4 ²⁵ process using TMP and LiO^tBu results in a reduction of carbon content from ~12% to <1%, as we find without the addition of the H_2O pulse the TMP will not fully react with the LiO^tBu -terminated surface ligands, resulting in carbon incorporation into the glass.

For the quaternary ALD process, we investigated $^p\text{N}_2$ dosing separately after each step of the process sequence. Of the numerous permutations of dose sequences possible, we find that N doping of the films is possible with only one specific dose sequence, as most of the surface terminating ligands are nonreactive toward $^p\text{N}_2$. We managed to incorporate nitrogen into the ALD films *only* when the $^p\text{N}_2$ was applied after the TMP pulse, directly before the LiO^tBu pulse.

The full quaternary ALD LiPON process sequence (Scheme 1), monitored in real-time by *in-situ* spectroscopic ellipsometry (Figure 1), elucidates the impact of ligand chemistry on the

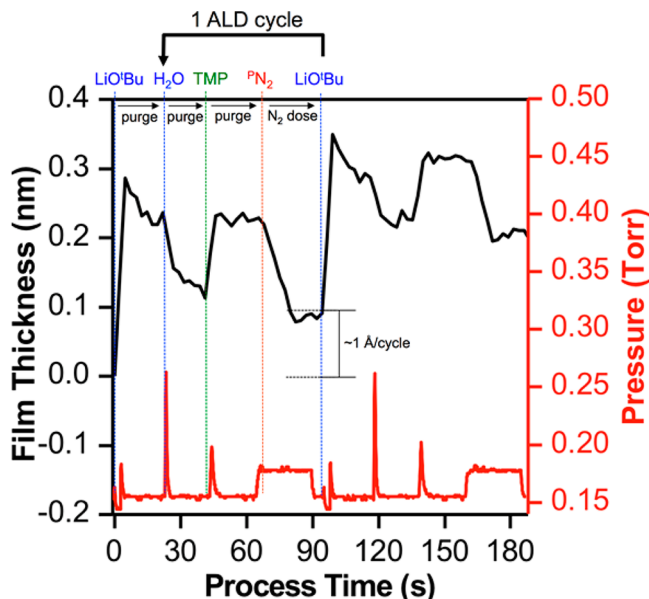


Figure 1. (left axis, black) *In-situ* ellipsometric monitoring of film growth during one complete LiPON ALD cycle. (right axis, red) Pressure trace in the ALD reactor showing corresponding precursor pulses during ALD growth.

ALD process sequence. Application of the $^p\text{N}_2$ dose in any other location during the process sequence resulted in deposition of nitrogen-free polycrystalline Li_3PO_4 , likely due to the nature of the nitrogen bonding in LiPON.²⁶ In doped phosphate glasses, nitrogen atoms serve as either doubly or triply coordinated bridges among phosphorus atoms. In the ALD process, incoming N ions presumably act to “crosslink” otherwise disparate TMP fragments on the surface, which we believe aids in the amorphization of the film. If the phosphorus atoms are not the surface species (such as after any other precursor pulse aside from TMP), then the stable bonding sites for N are unavailable due to steric hindrance from ligands on the other precursors, preventing incorporation of N into the ALD films.^{4,27}

Figure 1 compares the film thickness and pressure change through the optimized LiPON process cycle. The changes in film thickness are generally in line with the mechanism

proposed in Scheme 1. The addition of LiO^tBu species to the surface leads to a thickness gain of approximately 0.3 nm, which is reduced somewhat during the purge period due to a combination of vaporization and decomposition. The measured thickness sharply decreases upon the addition of H_2O , which is consistent with a reaction liberating *tert*-butanol and leaving behind the smaller LiOH unit (Scheme 1, b to c). The addition of TMP again increases the thickness of the film consistent with a stable, surface bound methyl phosphate species. Finally, the application of a remote N_2 plasma coincides with a linear decrease of film thickness, which is consistent with the cross-linking reaction proposed in Scheme 1, steps d to e. We note that while the N_2 plasma is a remote process, some high energy ions and neutrals may be reaching the film and etching the surface, although the overall growth rate is clearly positive in all cases.

Figure 2 shows high-resolution XPS spectra of the ALD LiPON films demonstrating the impact of the $^p\text{N}_2$ dose on the binding environment of the ALD films. Due to the lack of carbon in these films (Supporting Information), all spectra are calibrated against the Li 1s peak, set at 55.6 eV in line with previously measured values for Li_3PO_4 .²⁸ The Li 1s orbital generally shows the least variation of binding energy with chemical environment among the elements present, warranting its choice for use in calibration. With no $^p\text{N}_2$ dose the O 1s (531.6 eV) and P 2p 3/2 (133.6 eV) XPS peaks are also consistent with Li_3PO_4 . As the $^p\text{N}_2$ dose is increased, the chemistry of the film changes markedly. The overall incorporation of N grows with dose time. The N spectrum demonstrates two chemical species, which are generally associated with atoms linking either two or three P atoms in the glass.²⁹ There is a slight shift of the phosphate O 1s peak to lower binding energies by ~0.1 eV, along with the emergence of a second O 1s peak at 533.0 eV, attributed to an increase in bridging oxygen (P—O—P) in the LiPON glass. Interestingly, the parallel increase of both the bridging oxygen and nitrogen content stands in contrast with previous reports on the chemistry of sputtered LiPON films,³⁰ in which more N results in less bridging oxygen. We believe this is due to the fact that sputtered LiPON is usually amorphous regardless of N content and so contains a maximum number of bridging oxygens when no nitrogen is present to substitute for them. In our case, the film is also undergoing a transition from crystalline to amorphous with increasing N content, and so the overall number of all bridging species is increasing. Both P 2p peaks are slightly broadened with increasing N content, also consistent with LiPON amorphization with higher $^p\text{N}_2$ dose, as will be demonstrated below.

Despite the varying $^p\text{N}_2$ dose during the ALD process, we find that the growth rate is relatively stable around 1.05 Å/cycle, as shown in Figure 3a. The slope of the fit to the growth rate is within experimental error. Figure 3b demonstrates that the ratio of doubly coordinated N to triply coordinated N in the ALD LiPON is consistent with increasing N dose, indicating that, as the N content is increased, the doping environment of the LiPON is chemically similar. This specific ratio of triply coordinated N to doubly coordinated N is likely due to our use of a single energy remote plasma to nitrogenate the films. Modification of the N radical energy in the plasma could likely modify this ratio; however, we are limited by our instrumentation capabilities. The elemental ratios of the ALD LiPON films as determined by XPS are plotted in Figure 3c. As the $^p\text{N}_2$ dose is increased, ALD films transition from

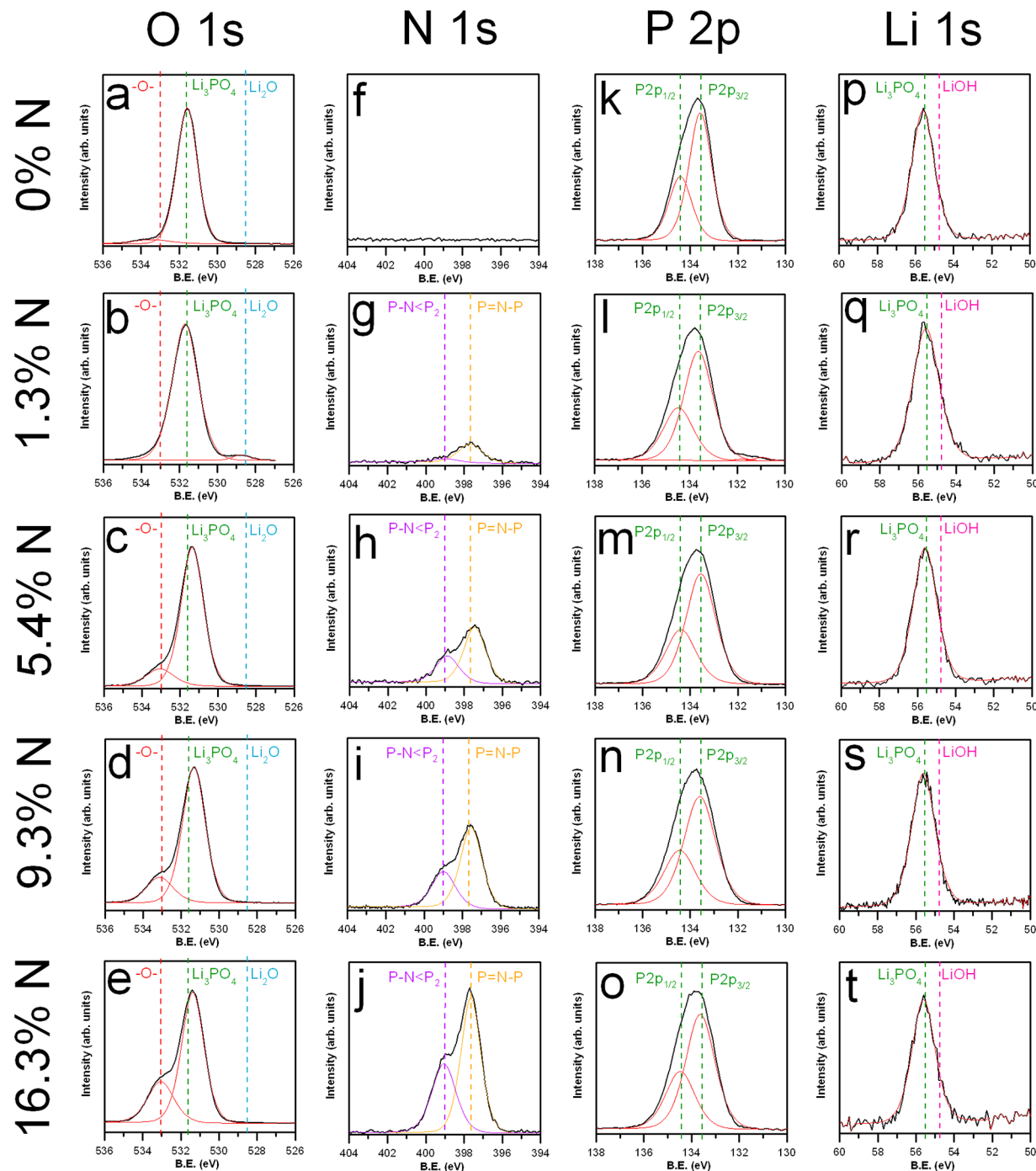


Figure 2. In-situ high-resolution core-level XPS spectra (columns) of as-deposited ALD LiPON at 250 °C demonstrating nitrogen doping as a function of N₂ pulse time (rows). Spectra include deconvolution of multicomponent peaks.

polycrystalline Li₃PO₄ to amorphous LiPON, as indicated by the XRD data in Figure 3d. This transition point occurs near 4.5% N content, as ALD LiPON deposited with a 5 s ¹⁵N₂ dose remains polycrystalline, while ALD LiPON deposited with a 10 s ¹⁵N₂ dose is amorphous. To verify that this effect was due to the nitrogen content of the films and not the plasma dose, we ran an ALD LiPON process using an Ar plasma instead of the usual N₂ plasma step, resulting in the deposition of polycrystalline Li₃PO₄ films. Clearly, this indicates that LiPON amorphization is due to inclusion of N in glass forming networks and not as a result of the ¹⁵N₂ dose.

AFM height maps of ALD LiPON films 40 nm thick with 1.8% N content (Figure 4a) and 16.3% N content (Figure 4b) clearly demonstrate this crystalline to amorphous transition with increasing N content of the ALD films. The RMS roughness of these films is 10.1 nm for the 1.8% N LiPON film and 0.78 nm for the 16.3% N LiPON film, respectively. SEM images of the same samples are also presented in Figure 4c,d, showcasing the film texture. Note that the SEM image of the amorphous ALD LiPON film in Figure 4c shows no distinct features due to the high quality amorphous material. This crystalline to amorphous transition differs from previous results which found that sputter deposited Li₃PO₄ exposed to a high

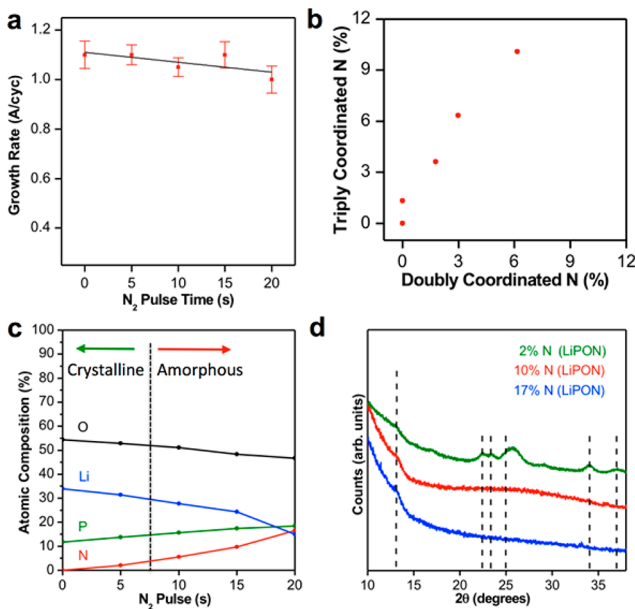


Figure 3. (a) Growth rate as a function of $\text{P}^{\text{N}}\text{N}_2$ dose for ALD LiPON. (b) Ratio of doubly coordinated N to triply coordinated N in the LiPON structure as determined by XPS, indicating a uniform bonding environment as a function of N content. (c) Film stoichiometry as determined by peak fitting the high-resolution XPS peaks in Figure 2. (d) XRD data of 50 nm thick LiPON thin films demonstrating the crystalline to amorphous transition with increasing nitrogen content.

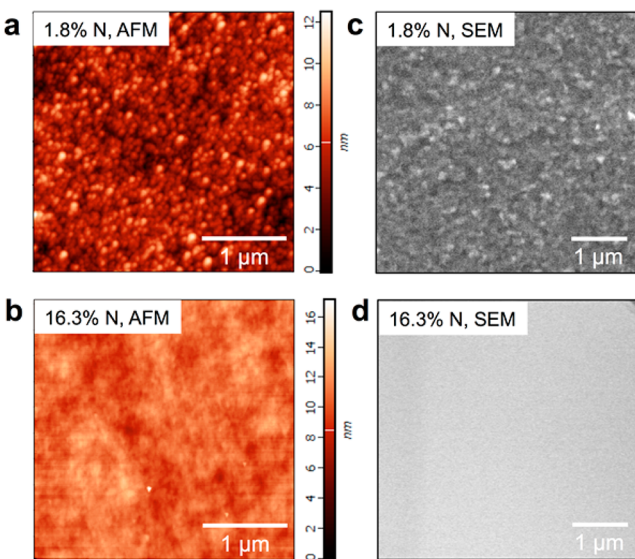


Figure 4. AFM height maps of (a) LiPON film with 1.8% N and (b) LiPON film with 16.3% N. (c) and (d) show SEM images of the same films in (a) and (b) to illustrate film texture.

energy N_2 plasma discharge exhibited an amorphous to crystalline transition with increasing N content; however, this is perhaps not surprising considering the drastically different deposition techniques.¹¹

One of the hallmarks of the ALD process is the ability to conformally coat high aspect ratio nanostructures with thin, uniform layers. Here, we deposited ALD LiPON films with varied N content on MWCNT sponge scaffolds^{13,16} for both morphological imaging and ellipsometric thickness calibration. TEM images of MWCNTs covered with ALD LiPON films are

shown in Figure 5. The morphology of these LiPON films is consistent with the AFM and SEM data presented in Figure 4

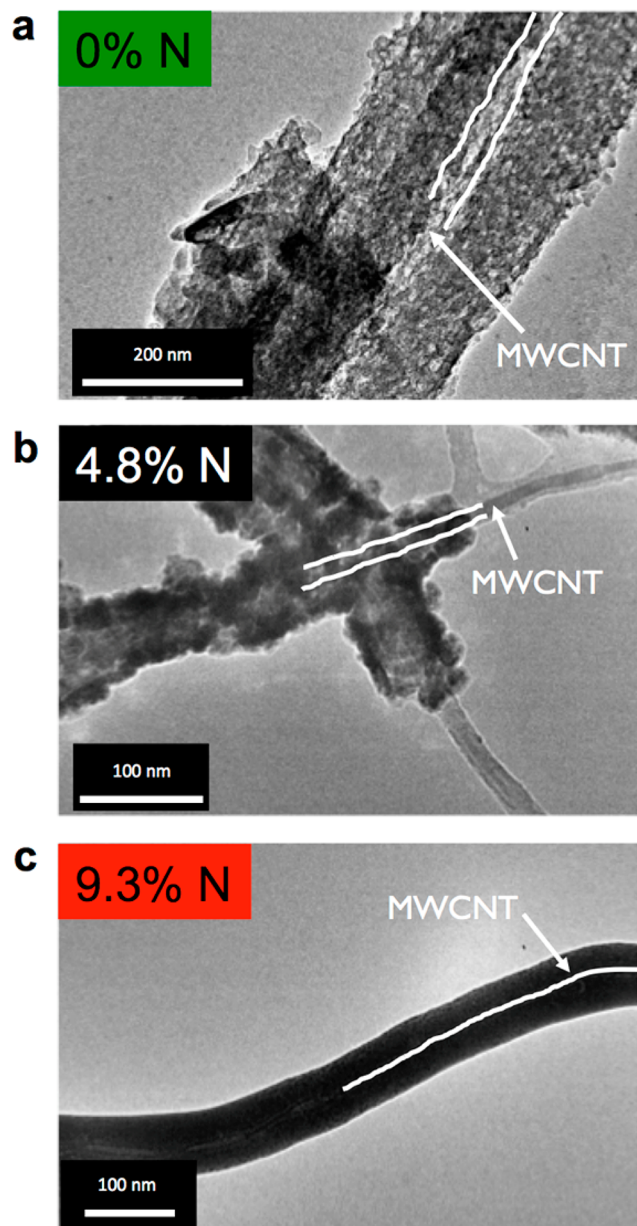


Figure 5. TEM images of ALD LiPON deposited on a MWCNT sponge with (a) 0% N, (b) 4.8% N, and (c) 9.3% N content. Both (a) and (b) are polycrystalline, while (c) is amorphous. The diameter of the MWCNTs is 30–40 nm.

and clearly demonstrates the uniform deposition possible on high aspect ratio scaffolds through the ALD process. Notably, we find that while crystalline ALD LiPON is stable, amorphous ALD LiPON degrades rapidly upon electron beam exposure, preventing focused high-resolution imaging, consistent with others' observations.³¹

ELECTROCHEMICAL TESTING

We tested the ionic conductivity by deposition of ALD LiPON with various thicknesses and N contents onto stainless steel substrates, which were then assembled into CR2032 coin cells. Electrochemical impedance spectroscopy (EIS) tests on these

LiPON films as a function of film thickness, all with 5.5% N, are shown in Figure 6a. Using the circuit model for thin LiPON

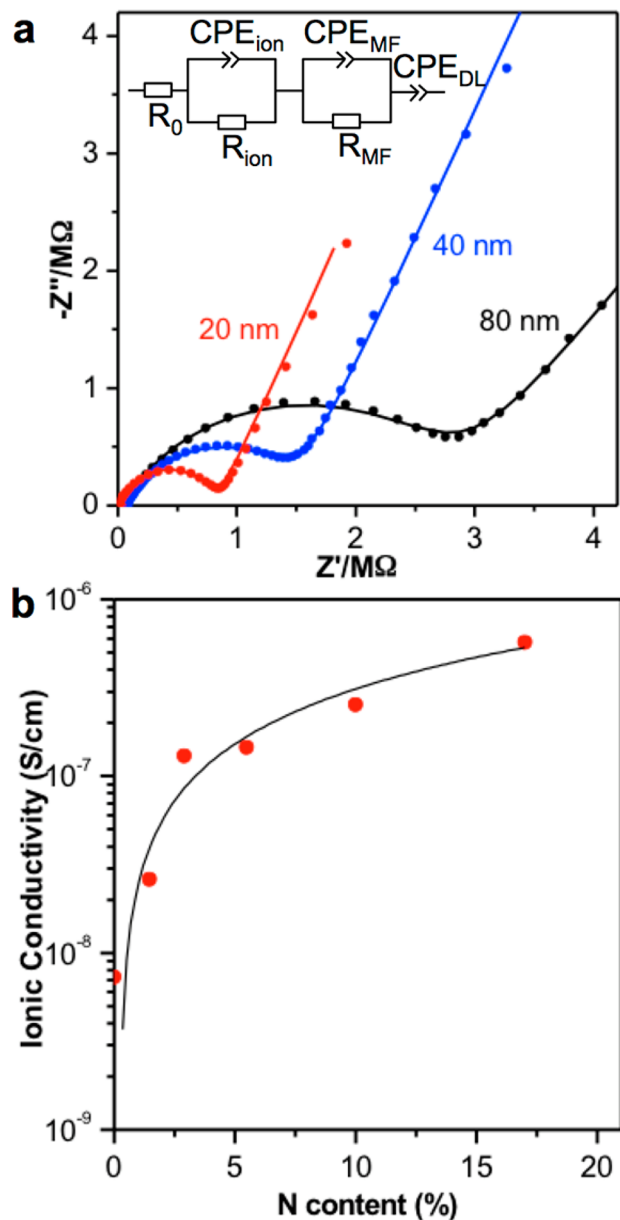


Figure 6. (a) EIS curves for 20, 40, and 80 nm thick ALD LiPON working electrodes in coin cells with a Li metal counter electrode. Dots are measured data, and lines are fits to the measured data using the inset circuit model used for impedance analysis adapted from Dudney.³² (b) Ionic conductivity of ALD LiPON films plotted as a function of N content along with linear fit to the data.

developed by Dudney (Figure 6a, inset),³² we determine the ionic conductivity to be $1.45 \times 10^{-7} \text{ S}/\text{cm} \pm 3 \times 10^{-7} \text{ S}/\text{cm}$, slightly lower than previously published results of sputter deposited LiPON with similar nitrogen content.³³ However, this value represents the highest conductivity of any ALD solid electrolyte reported to date.^{17,20,21} In Dudney's model, the ionic conduction is modeled by two parallel R/CPE circuit elements (frequency-dependent capacitors) at both high (CPE_{ion}/R_{ion}) and medium (CPE_{MF}/R_{MF}) frequencies. Each of these parallel circuit elements describes ionic conduction processes in the bulk of the LiPON and near the interface

regions, respectively. We calculate the ionic conductivity of the LiPON using R_{ion} . The EIS model contains two additional circuit elements: an electrode interface capacitance (CPE_{DL}) and contact/solution resistance (R_0). Dudney's model also includes a parallel resistor to model the electronic leakage current detected in very thin LiPON films. However, by evaluating the LiPON solid electrolyte in an organic liquid electrolyte environment, our EIS adds an electronically insulating electrolyte in series with two electrodes, eliminating the possibility of electronic leakage in our system. We note that the ionic conductivity does not change significantly with film thickness, and as such bulk ionic conductivity in the LiPON likely dominates over the interfacial impedance of ALD LiPON. Optimized circuit values of our fits to the data in Figure 6 are shown in Supporting Information.

The ionic conductivity of sputtered LiPON has been reported to increase with increasing N content,²⁹ and indeed we measure a dramatic increase in the ionic conductivity of the ALD LiPON with nitrogen content increasing from 1.8% to 16.3%, plotted in Figure 6b. For non-doped ALD Li_3PO_4 , we measure an ionic conductivity of $7.5 \times 10^{-9} \text{ S}/\text{cm}$, in the range of values previously measured for the ionic conductivity of Li_3PO_4 .³⁴

In order to demonstrate ALD LiPON's function in a model electrochemical system, LiPON films were applied to sputter-deposited amorphous silicon anodes on copper current collectors, as well as to the bare Cu current collector, in order to determine the influence of the ALD LiPON layers on lithiation behavior of the underlying silicon. CV scans of these anodes collected between 10 mV and 1.2 V vs Li/Li⁺ at 0.1 mV/s sweep rate are shown in Figure 7.

The ALD LiPON deposited directly on the Cu current collector (green) shows a lack of peaks in the CV, indicating a lack of redox reactions occurring during lithiation/delithiation of LiPON, as expected for an ionic capacitor. Notably, a

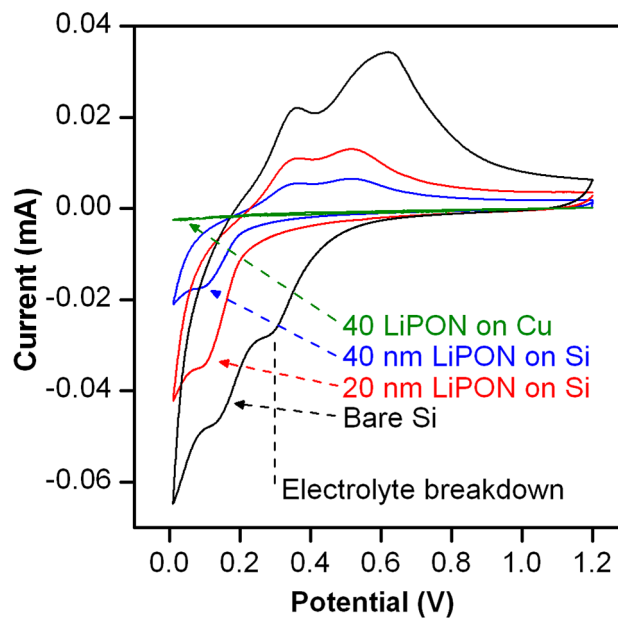


Figure 7. CV curves of (black) bare sputtered Si; (red) 20 nm ALD LiPON on sputtered Si; (blue) 40 nm ALD LiPON on sputtered Si; and (green) 40 nm ALD LiPON on Cu. The sweep rate for all CV scans was 0.1 mV/s in 1:1 EC:DEC with 1 M LiPF_6 electrolyte and a Li metal counter electrode.

cathodic current increase due to electrolyte reduction and SEI formation is not obtained even near 0 V vs. Li/Li⁺, suggesting the LiPON film is an effective barrier for electron transfer from the electrode to the organic electrolyte.

The uncoated silicon anode behaves electrochemically as expected, with two cathodic peaks associated with the organic electrolyte breakdown and lithiation of the silicon, at ~300 mV and ~180 mV, respectively.³⁵ Application of both 20 and 40 nm ALD LiPON coatings on the silicon completely extinguishes the cathodic peak associated with SEI formation. On the anodic scan, two peaks commonly associated with delithiation are seen for both uncoated and LiPON coated silicon.

Thicker LiPON layers do show a reduced current response to the applied potential sweep in both anodic and cathodic scan regions, indicating that the impedance of the coated anodes increases with increasing LiPON film thickness as expected.

CONCLUSIONS

We have demonstrated the first reported ALD process for the solid lithium electrolyte LiPON and shown the ability to modify the N content in the LiPON films from 0% to 16.3% N by variation of the nitrogen dose at a specific location in the ALD sequence.

The combination of highly tunable thickness during growth, tunable N content, and the ability to conformally deposit LiPON on high aspect ratio nanostructures is a desirable and very attractive combination for incorporating solid electrolyte layers onto challenging electrode geometries in both 3D solid state micro-/nanobatteries and as protection layers in metal anodes based beyond Li ion batteries.

ASSOCIATED CONTENT

Supporting Information

XPS survey spectra of ALD LiPON and tables of optimized circuit components from EIS fitting to the data shown in Figure 6. The Supporting Information is available free of charge on the ACS Publications website at DOI: 10.1021/acs.chemmater.Sb01654.

AUTHOR INFORMATION

Corresponding Author

*Alexander C. Kozen. E-mail: ackozen@umd.edu.

Author Contributions

The manuscript was written through contributions of all authors. All authors have given approval to the final version of the manuscript.

Notes

The authors declare no competing financial interest.

ACKNOWLEDGMENTS

This work was supported as part of the Nanostructures for Electrical Energy Storage (NEES), an Energy Frontier Research Center funded by the U.S. Department of Energy, Office of Science, Basic Energy Sciences, under Award Number DESC0001160. We acknowledge the support of the Maryland Nanocenter and its NispLab. M.N. acknowledges a postdoctoral fellowship through the Fulbright Program.

ABBREVIATIONS

LiPON, lithium phosphorus oxynitride; XPS, X-ray photoelectron spectroscopy; ALD, atomic layer deposition; AFM,

atomic force microscopy; SEM, scanning electron microscopy; TEM, transmission electron microscopy; IV, current–voltage; TMP, trimethylphosphate; LiO^tBu, lithium *tert*-butoxide; ^{PN}₂, nitrogen plasma; MOCVD, metal–organic chemical vapor deposition; EIS, electrochemical impedance spectroscopy; SEI, solid electrolyte interphase

REFERENCES

- (1) Rubloff, G. W.; Kozen, A. C.; Bok Lee, S. From nanoscience to solutions in electrochemical energy storage. *J. Vac. Sci. Technol., A* **2013**, *31*, 05S803.
- (2) Long, J.; Dunn, B.; Rolison, D.; White, H. Three-dimensional battery architectures. *Chem. Rev.* **2004**, *104*, 4463–4492.
- (3) Bates, J. B.; Dudney, N. J.; Gruzalski, G. R.; Zuhur, R. A.; Choudhury, A.; Luck, C. F.; Robertson, J. D. Fabrication and Characterization of Amorphous Lithium Electrolyte Thin-Films and Rechargeable Thin-Film Batteries. *J. Power Sources* **1993**, *43*, 103–110.
- (4) Knauth, P. Inorganic solid Li ion conductors: An overview. *Solid State Ionics* **2009**, *180*, 911–916.
- (5) West, W. C.; Whitacre, J. F.; Lim, J. R. Chemical stability enhancement of lithium conducting solid electrolyte plates using sputtered LiPON. *J. Power Sources* **2004**, *126*, 134–138.
- (6) Belous, A. G.; V'yunov, O. I.; Kovalenko, L. L.; Bohnke, O.; Bohnke, C. Synthesis of thin-film electrodes based on LiPON and LiPON-LLTO-LiPON. *Russ. J. Electrochim.* **2014**, *50*, 523–530.
- (7) Dudney, N. J. Addition of a thin-film inorganic solid electrolyte (Lipon) as a protective film in lithium batteries with a liquid electrolyte. *J. Power Sources* **2000**, *89*, 176–179.
- (8) Li, J.; Baggetto, L.; Martha, S. K.; Veith, G. M.; Nanda, J.; Liang, C.; Dudney, N. J. An Artificial Solid Electrolyte Interphase Enables the Use of a LiNi_{0.5}Mn_{1.5}O₄ SV Cathode with Conventional Electrolytes. *Adv. Energy Mater.* **2013**, *3*, 1275–1278.
- (9) Nowak, S.; Berkemeier, F.; Schmitz, G. Ultra-thin LiPON films - Fundamental properties and application in solid state thin film model batteries. *J. Power Sources* **2015**, *275*, 144–150.
- (10) Ruzmetov, D.; Oleshko, V. P.; Haney, P. M.; Lezec, H. J.; Karki, K.; Baloch, K. H.; Agrawal, A. K.; Davydov, A. V.; Krylyuk, S.; Liu, Y.; Huang, J.; Tanase, M.; Cumings, J.; Talin, A. A. Electrolyte Stability Determines Scaling Limits for Solid-State 3D Li Ion Batteries. *Nano Lett.* **2012**, *12*, 505–511.
- (11) Kim, Y. G.; Wedley, H. N. G. The influence of the nitrogen-ion flux on structure and ionic conductivity of vapor deposited lithium phosphorus oxynitride films. *J. Power Sources* **2011**, *196*, 1371–1377.
- (12) Kim, H. T.; Mun, T.; Park, C.; Jin, S. W.; Park, H. Y. Characteristics of lithium phosphorous oxynitride thin films deposited by metal-organic chemical vapor deposition technique. *J. Power Sources* **2013**, *244*, 641–645.
- (13) Chen, X.; Zhu, H.; Chen, Y.-C.; Shang, Y.; Cao, A.; Hu, L.; Rubloff, G. W. MWCNT/V2O₅ Core/Shell Sponge for High Areal Capacity and Power Density Li-Ion Cathodes. *ACS Nano* **2012**, *6*, 7948–7955.
- (14) Gerasopoulos, K.; Chen, X.; Wang, C.; Culver, J.; Ghodssi, R. Self-assembled Ni/TiO₂ nanocomposite anodes synthesized via electroless plating and atomic layer deposition on biological scaffolds. *Chem. Commun.* **2010**, *46*, 7349.
- (15) Knoops, H. C. M.; Donders, M. E.; van de Sanden, M. C. M.; Notten, P. H. L.; Kessels, W. M. M. Atomic layer deposition for nanostructured Li-ion batteries. *J. Vac. Sci. Technol., A* **2012**, *30*, 010801.
- (16) Gregorczyk, K. E.; Kozen, A. C.; Chen, X.; Schroeder, M. A.; Noked, M.; Cao, A.; Hu, L.; Rubloff, G. W. Fabrication of 3D Core–Shell Multiwalled Carbon Nanotube@RuO₂ Lithium-Ion Battery Electrodes through a RuO₂ Atomic Layer Deposition Process. *ACS Nano* **2015**, *9* (1), 464–473.
- (17) Aaltonen, T.; Alnes, M.; Nilsen, O.; Costelle, L.; Fjellvåg, H. Lanthanum titanate and lithium lanthanum titanate thin films grown by atomic layer deposition. *J. Mater. Chem.* **2010**, *20*, 2877–2881.

- (18) Hamalainen, J.; Holopainen, J.; Munnik, F.; Hatanpaa, T.; Heikkila, M.; Ritala, M.; Leskela, M. Lithium Phosphate Thin Films Grown by Atomic Layer Deposition. *J. Electrochem. Soc.* **2012**, *159*, A259–A263.
- (19) Comstock, D. J.; Elam, J. W. Mechanistic Study of Lithium Aluminum Oxide Atomic Layer Deposition. *J. Phys. Chem. C* **2013**, *117*, 1677–1683.
- (20) Aaltonen, T.; Nilsen, O.; Magraso, A.; Fjellvåg, H. Atomic Layer Deposition of Li₂O-Al₂O₃ Thin Films. *Chem. Mater.* **2011**, *23*, 4669–4675.
- (21) Perng, Y.-C.; Cho, J.; Sun, S. Y.; Membreno, D.; Cirigliano, N.; Dunn, B.; Chang, J. P. Synthesis of ion conducting LixAl_ySizO thin films by atomic layer deposition. *J. Mater. Chem. A* **2014**, *2*, 9566–9573.
- (22) Kozen, A. C.; Schroeder, M. A.; Osborn, K. D.; Lobb, C. J.; Rubloff, G. W. Examining the role of hydrogen in the electrical performance of in situ fabricated metal-insulator-metal trilayers using an atomic layer deposited Al₂O₃ dielectric. *Appl. Phys. Lett.* **2013**, *102*, 173501.
- (23) Yeh, J. J.; Lindau, I. Atomic subshell photoionization cross sections and asymmetry parameters: 1. At. Data Nucl. Data Tables **1985**, *32*, 1–155.
- (24) Kozen, A. C.; Pearse, A. J.; Lin, C.-F.; Schroeder, M. A.; Noked, M.; Lee, S. B.; Rubloff, G. W. Atomic Layer Deposition and in Situ Characterization of Ultraclean Lithium Oxide and Lithium Hydroxide. *J. Phys. Chem. C* **2014**, *118*, 27749–27753.
- (25) Hamalainen, J.; Holopainen, J.; Munnik, F.; Hatanpaa, T.; Heikkila, M.; Ritala, M.; Leskela, M. Lithium Phosphate Thin Films Grown by Atomic Layer Deposition. *J. Electrochem. Soc.* **2012**, *159*, A259–A263.
- (26) Roh, N. S.; Lee, S. D.; Kwon, H. S. Effects of deposition condition on the ionic conductivity and structure of amorphous lithium phosphorus oxynitrate thin film. *Scr. Mater.* **1999**, *42*, 43–49.
- (27) Mascaraque, N.; Tricot, G.; Revel, B.; Durán, A.; Muñoz, F. Nitrogen and fluorine anionic substitution in lithium phosphate glasses. *Solid State Ionics* **2014**, *254*, 40–47.
- (28) Morgan, W. E.; Van Wazer, J. R.; Stec, W. J. Inner-orbital photoelectron spectroscopy of the alkali metal halides, perchlorates, phosphates, and pyrophosphates. *J. Am. Chem. Soc.* **1973**, *95*, 751–755.
- (29) Mascaraque, N.; Fierro, J.; Durán, A.; Muñoz, F. An interpretation for the increase of ionic conductivity by nitrogen incorporation in LiPON oxynitride glasses. *Solid State Ionics* **2013**, *233*, 73–79.
- (30) Fleutot, B.; Pecquenard, B.; Martinez, H.; Letellier, M.; Levasseur, A. Investigation of the local structure of LiPON thin films to better understand the role of nitrogen on their performance. *Solid State Ionics* **2011**, *186*, 29–36.
- (31) Zheng, H.; Liu, Y.; Mao, S. X.; Wang, J.; Huang, J. Y. Beam-assisted large elongation of in situ formed Li₂O nanowires. *Sci. Rep.* **2012**, *2*, 542.
- (32) Li, J.; Dudney, N. J.; Nanda, J.; Liang, C. Artificial Solid Electrolyte Interphase To Address the Electrochemical Degradation of Silicon Electrodes. *ACS Appl. Mater. Interfaces* **2014**, *6*, 10083–10088.
- (33) Yu, X.; Yu, X.; Bates, J. B.; G E Jellison, J.; Hart, F. X. A stable thin-film lithium electrolyte: Lithium phosphorus oxynitride. *J. Electrochem. Soc.* **1997**, *144*, 524–532.
- (34) Xie, J.; Oudenoven, J. F. M.; Harks, P. P. R. M. L.; Li, D.; Notten, P. H. L. Chemical Vapor Deposition of Lithium Phosphate Thin-Films for 3D All-Solid-State Li-Ion Batteries. *J. Electrochem. Soc.* **2014**, *162*, A249–A254.
- (35) McDowell, M. T.; Lee, S. W.; Nix, W. D.; Cui, Y. 25th Anniversary Article: Understanding the Lithiation of Silicon and Other Alloying Anodes for Lithium-Ion Batteries. *Adv. Mater.* **2013**, *25*, 4966–4985.